31/2

ISSN 0234-5366

ОБЪЕДИНЕННЫЙ
ИНСТИТУТ
ЯДЕРНЫХ
ИССЛЕДОВАНИЙ

JOINT INSTITUTE
FOR NUCLEAR
RESEARCH

1[64]-94

КРАТКИЕ СООБЩЕНИЯ ОИЯИ

JINR RAPID COMMUNICATIONS

ДУБНА

Объединенный институт ядерных исследований
Joint Institute for Nuclear Research

1 [64] -94

КРАТКИЕ СООБЩЕНИЯ ОИЯИ
JINR RAPID COMMUNICATIONS

сборник
collection

Дубна 1994

ОГЛАВЛЕНИЕ
CONTENTS

УДК 539.142

ON PLANE NUCLEAR VORTEX

V.G.Kartavenko, V.V.Pupyshev, P.Quentin*

We analyze the pure vortical motion in nuclear systems excluding the usual approximation on smallness of the excitation amplitude and the additional assumptions on the shape of a nuclear system. The equations to describe a nonlinear plane nuclear vortex are presented in the frame of nuclear hydrodynamics. The evolution of the shape of a vortex is analogous to a propagation of a nonlinear dispersion wave in a plane. These states can be considered as a generalization of elliptic Kirchhoff vortex. We have proved that the solutions having the symmetry relative to the turn by an angle $2\pi/l$ with integer parameter $l = 2, 3, 4\ldots$ can exist. These vortexes seem to be two-dimensional analogues to the rotating nuclear systems having stable quadrupole, octupole, hexadecupole deformations accordingly.

The investigation has been performed at the Bogoliubov Laboratory of Theoretical Physics, JINR.

О плоском ядерном вихре

В.Г.Картавенко, В.В.Пупышев, Ф.Кантен

Чисто вихревое движение в ядерных системах анализируется без использования обычных приближений о малости амплитуды возбуждения и добавочных предположений о форме ядерной системы. В рамках ядерной гидродинамики представлены основные уравнения для описания плоских нелинейных ядерных вихрей. Эволюция формы вихря аналогична распространению в плоскости нелинейной дисперсной волны. Эти состояния могут быть рассмотрены как обобщение эллиптических вихрей Кирхгофа. Показано, что могут существовать решения, имеющие симметрию относительно поворота на угол $2\pi/l$ с целым параметром $l = 2, 3, 4\ldots.$ Эти вихри могут быть двумерными аналогами вращающихся ядерных систем, имеющих соответственно стабильную квадрупольную, октупольную, гексадекапольную... деформации.

Работа выполнена в Лаборатории теоретической физики им.Н.Н.Боголюбова ОИЯИ.

1. Introduction

Rotating states were always in the focus of attention of theoretical and experimental physics [1]. High spin states (e.g., see [2] and reference therein) is the most popular type of the vortical motion in nuclear systems, but

*Centre D'Etudes Nucleaires de Bordeaux Gradignan, IN2P3-CNRS
BP 120, 33175 Gradignan Cedex, France

far from being the only possible one. Many attempts were undertaken to find topological nontirival vortical states. Vortical isomer nuclei were supposed to exist [3] (the superconduction component of the nuclear fluid with the quantum curl was oriented along the symmetry axis of a rotating drop). Not long ago a supposition close in the physical sense to the above was mentioned again [4]. It was shown that superfluidity caused by triplet Cooper pairing makes the nuclear liquid anisotropic and also leads to discrete rotational spectra at high excitation energies [5]. The approximate solution to describe stable vortexes was obtained in the framework of the liquid drop model. In the first case, the solutions corresponded to the «hot spot», emerged in peripheral collisions [6]. In the second case, the soliton type solutions on a nuclear surface were associated with a cluster type configuration [7], [8]. The analogy with the admixture electrons and positrons in dense gases [9], [10] allows us to suppose the existence of the vortical «rings» on admixture hadrons in nuclear systems.

Recently, nuclear theory has predicted the formation of the new exotic vortical objects such as «disks» [11], [12], unstable hollow «bubbles» and «rings» [13] which decay by intermediate mass emission.

In this report we analyse the pure vortical motion excluding the usual approximation on smallness of the excitation amplitude and the additional assumptions on the shape of the nuclear system.

In Sec.2 the basic equations to describe plain nuclear vortex are presented within the nuclear hydrodynamics. Qualitative analysis of the main features of a vortes is done in Sec.3. Symmetry of the solutions is considered in Sec.4. It is shown that there probably exists the possibility to derive the stable solutions having the symmetry relative to the turn by an angle $2\pi/l$ with the integer parameter $l = 2, 3, 4\ldots$ Last Section contains a short symmary.

2. Basic Equations

We use the semiclassical nuclear hydrodynamics based on the current $\hat{j}$ and density $\hat{\rho}$ algebra and hydrodynamic representation for the nuclear hamiltonian, which is equivalent in view of the equations of motion for $\hat{j}$ and $\hat{\rho}$ to the initial hamiltonian. Gradient terms of the «pressure» drop out from the equations of motion on separating the curl component of the velocity field and the equations of motion for rot v are formally reduced to the pure kinematic form, at least for the Skyrme type forces.

For an incompressible $(\rho \equiv \rho_0)$ nuclear vortical flow it is convenient to turn to the vorticity ζ and the vector potential **A**

$$\mathbf{v} = \mathrm{rot}\,\mathbf{A}, \qquad \mathrm{div}\,\mathbf{A} = 0, \qquad \frac{\partial}{\partial t}\zeta + v_r\frac{\partial}{\partial r}\zeta + v_\phi\frac{1}{r}\frac{\partial}{\partial \phi}\zeta = 0,$$

$$\zeta = \text{rot } \mathbf{v} = \text{rot rot } \mathbf{A} = \text{grad div } \mathbf{A} - \Delta\mathbf{A} = -\Delta\mathbf{A}.$$

We restict ourselves to the simplest rotational flow, two-dimensional motion $v(r, \phi) = v_r\mathbf{e}_r + v_\phi\mathbf{e}_\phi$, $\mathbf{A} = A\mathbf{e}_z$, $\zeta = \zeta\mathbf{e}_z$, where (r, ϕ) are polar coordinates of a point. The velocity projections v_r, v_ϕ can be determined by differentiating $A(r, \phi)$ with respect to r and ϕ: $v_r(r, \phi) = r^{-1}\partial A/\partial\phi$, $v_\phi(r, \phi) = -\partial A/\partial r$. The current function $A(r, \phi)$ can be derived from the Poisson equation by the two-dimensional Green function for the Laplace operator $\mathrm{A}(r, \phi) = (2\pi)^{-1}\int d\phi' dr' r' \ln(|\mathbf{r} - \mathbf{r}'|)\,\zeta(r', \phi')$.

In this report we consider two-dimensional analogues of the nuclear «disks» — plane nuclear vortexes — a new type of a pure vortical state of incompressible nuclear matter. They are the finite areas of the constant vorticity on a plane $\zeta(r', \phi', t) \equiv \zeta_0$ within the uniform-rotating contour $\Gamma(r, \phi) \equiv r - R(\phi) = 0$. In essence, these states can be considered as the generalization of the elliptic Kirchhoff vortex [14]. The dynamical condition on the contour $(\mathbf{n}\cdot\mathbf{v}) = (\mathbf{n}\cdot\mathbf{v}_{\text{contour}})$ and the normal vector n are given by

$$\mathrm{n} = \frac{\sigma\nabla\Gamma}{|\nabla\Gamma|} = \sigma\,(\mathbf{e}_r - S(\phi)\,\mathbf{e}_\phi)\,(1 + S(\phi)^2)^{-1/2}, \qquad S(\phi) \equiv \frac{1}{R}\frac{dR}{d\phi},$$

$$\Omega\frac{dR}{d\phi} + v_r - v_\phi\left(\frac{1}{R}\frac{dR}{d\phi}\right) = 0,$$

where Ω is an angular velocity of the uniform-rotation of the contour and $\sigma = \pm 1$ defines the orientation of the contour.

Finally the equatin for the vortex boundary may be cast into the form of the following one-dimensional nonlinear integro-differential equation

$$\frac{2\pi\Omega}{\zeta_0}\frac{dR}{d\phi} = \int_0^{2\pi} d\phi' R((\phi') \ln(|\delta\mathbf{R}|)\,[(1 + S(\phi)\,S(\phi'))\sin(\phi' - \phi) +$$
$$+ (S(\phi) - S(\phi'))\cos(\phi' - \phi)],$$

where $|\delta\mathbf{R}| = (R(\phi)^2 + R(\phi')^2 - 2R(\phi)\,R(\phi')\cos(\phi - \phi'))^{1/2}$.

3. Qualitative Analysis

For a quantitative analysis of the Eq. (1) it is necessary to build its discrete analogue, that is, in progress. Here we shall present only the qualitative analysis which can be done by analogy with the well-known elliptic Kirchhoff vortex and the solution for small perturbations of the circle [14].

(i) Despite the internal part of the vortex is rotating with a constant angular velocity, this motion differs from the motion of a rigid body, as the contour is rotating with a different velocity, more slowly.

The small rotationless perturbation of a circle $\delta A(r, \phi) = \alpha\, (\zeta_0/2)\, R_0^2 (r/R_0)^l \cos(l\phi - \omega t)$, where l is an integer, gives us the following contour equation $R(\phi) = R_0(1 + \alpha \cos(l\phi - \omega t))$ (for $\alpha << R_0$). So the small perturbation given by trigonometrical functions, is a crimp moving along the circle vortex with the angular velocity $\Omega = \omega/l = (l - 1)\, \zeta_0/2l$. At $l = 2$ the perturbed shape is an ellipse, rotating about its center with the angular velocity $\zeta_0/4$, that is half of the velocity of the fluid into the contour. Perturbations of the higher symmetry $l \geq 3$ are rotating still slower.

(ii) The fixed ratio Ω/ζ_0 and the symmetry of states define completely the shape of the contour (for instance, for the elliptic vortex its eccentricity $\Omega/\zeta_0 = \varepsilon(1 + \varepsilon)^{-2}$.

Eq. (1) together with the definition of the velocity fields will describe the motion of the contour as the propagation of a nonlinear dispersion wave on a plane. At the beginning the moving contour will be inevitably distorted. However, if this state is stable, then the interference between the nonlinearity and the dispersion will lead to the return of the initial contour shape. If one could prove the existence of these states, then these vortexes will be an analogue of the solitons on a plane*.

(iii) The parameter Ω/ζ_0 will be the bifurcation parameter and will determine the vortex's stability. The integrals of motion are the square of the «disk» which is a two-dimensional analogue of the particle number and the circulation of the vortex defined by ζ_0. If the contour motion is unstable, one may expect the disintegration of the «disk» into the separate rotating vortexes and into the vortex filaments — two-dimension analogues of the rotating intermediate mass fragments.

In the next Sec. we will focus our attention on a symmetry of the solutions to Eq. (1).

4. Periodic Solutions

When $\alpha << R_0$, a contour velocity depends on the symmetry of a perturbation and the solutions may be classified by the parameter $l = 2, 3, 4\ldots$, or by the symmetry relative to the turn by the angle $2\pi/l$. Here we shall show

---

*For a last decade history of a soliton concept in nonrelativistic nuclear physics see review [15].

that the solutions having a symmetry relative to the turn by the angle $2\pi/l$ can exist. We do not use any additional approximation on smallness of the excitation amplitude.

Let us prove that the periodic solutions of Eq. (1) can exist at the class of $C^1_{[0,2\pi]}$ functions.

Eq. (1) may be cast in the following form

$$\frac{\partial}{\partial\phi}R(\phi) = \int_0^{2\pi} d\phi' F(R(\phi), R(\phi'), \phi, \phi'). \tag{2}$$

The necessary condition for an existence of the periodic solutions

$$R(\phi + T) = R(\phi), \qquad T = 2\pi/l, \qquad l = 1, 2, 3\ldots \tag{3}$$

is the periodicity of the right-hand side of Eq. (2), i.e.

$$\int_0^{2\pi} d\phi' F(R(\phi + T), R(\phi'), \phi + T, \phi') = \\ = \int_0^{2\pi} d\phi' F(R(\phi), R(\phi'), \phi, \phi'), \tag{4}$$

because for the periodic function (3) the left-hand side of this equation is a periodic one

$$\frac{\partial}{\partial\phi}R(\phi + T) = \frac{\partial}{\partial\phi}R(\phi). \tag{5}$$

Let us prove the afore-said necessary condition. Let $R(\phi)$ be a solution of Eq. (2) with the property (3). Then from Eqs. (1), (3), (5) one has the equalities

$$S(\phi + T) = S(\phi), \quad |\delta\mathbf{R}|^2(\phi + T, \phi' + T) = |\delta\mathbf{R}|^2(\phi, \phi'). \tag{6}$$

Further the following obvious identities will be also needed

$$\begin{aligned} \sin(\phi + T + \phi') &= \sin(\phi - (\phi' - T)), \\ \cos(\phi + T + \phi') &= \cos(\phi - (\phi' - T)). \end{aligned} \tag{7}$$

The left-hand side of Eq. (4) can be decomposed as the sum of the integrals

$$\int_0^{2\pi} \ldots = \int_0^T \ldots + \int_T^{2T} \ldots + \ldots + \int_{(2l-1)T}^{2\pi} \ldots \tag{8}$$

Let us consider the first one and reduce it to the other. Taking into account Eqs. (3), (5), (6) one has

$$\int_0^T d\phi' R(\phi')\,(1/2)\ln\left(R^2(\phi) + R^2(\phi') - 2R(\phi)\,R(\phi')\cos(\phi + T + \phi')\right)\times$$
$$\times\left(\sin(\phi + T \pm \phi')\,(1 + S(\phi)\,S(\phi')) + \right.$$
$$\left. + \cos(\phi + T - \phi')\,(S(\phi) - S(\phi'))\right). \qquad (9)$$

By replacement of the variables $t \equiv \phi' - T$, and $\phi = t + T$ integral (9) is written as

$$\int_{-T}^{0} dt(1/2)\ln\left(R^2(\phi) + R^2(t) - 2R(\phi)\,R(t)\cos(\phi - t)\right)\times$$
$$\times\left(\sin(\phi - t)\,(1 + S(\phi)\,S(t)) + \cos(\phi - t)\,(S(\phi) - S(t))\right). \qquad (10)$$

Analogously each integral $\int_{mT}^{(m+1)T} \ldots$ of the sum (8) is reduced to the following integral

$$\int_{(m-1)T}^{mT} d\phi' F(R(\phi), R(\phi'), \phi, \phi'), \qquad m = 1, \ldots, n - 1. \qquad (11)$$

Thus the following equalities are proved for $m = 1, \ldots, n - 1$

$$\int_{mT}^{(m+1)T} d\phi' F(R(\phi + T), R(\phi'), \phi + T, \phi') =$$
$$= \int_{(m-1)T}^{mT} d\phi' F(R(\phi), R(\phi'), \phi, \phi'). \qquad (12)$$

Consequently in order to prove the equality (4) one has to show that the following relation is fulfilled for the integral (10)

$$\int_{-T}^{0} dt\, R(t)\,(1/2)\ln((R^2(\phi) + R^2(t) - 2R(\phi)\,R(t)\cos(\phi - t))\times$$
$$\times\left(\sin(\phi - t)\,(1 + S(\phi)\,S(t)) + \cos(\phi - t)\,(S(\phi) - S(t))\right) =$$
$$= \int_{(n-1)T}^{nT=2\pi} dt\, R(t)\,(1/2)\ln((R^2(\phi) + R^2(t) - 2R(\phi)\,R(t)\cos(\phi - t))\times$$
$$\times\left(\sin(\phi - t)\,(1 + S(\phi)\,S(t)) + \cos(\phi - t)\,(S(\phi) - S(t))\right).$$

It is obvious because at a circle $R = R_0 =$ const an arc $-T \le \phi \le 0$ coincides with an arc $(n - 1)\,T \le \phi \le 2\pi$.

So Eq. (4) ensues from Eq. (3).

Let us present the periodic solutions for the two utmost cases:

i) $n = 1$, then $R(0) = R(2\pi)$ and $R(\phi)$ is just a general solution.

ii) $n = \infty$, then $R(\phi) = R(\phi + \delta\phi)$ for any small $\delta\phi$, i.e. $R(\phi) = \text{const}$ is a circle.

Let us test that a circle $R = R_0$ is a solution of Eq.(1). One has $\frac{\partial}{\partial\phi} R = 0$, $S = 0$, and Eq.(1) turns a following equality which can be proved.

$$0 = \int_0^{2\pi} dt\, R_0(1/2) \ln(R_0^2 + R_0^2 - 2R_0^2\cos(\phi - t)) \sin(\phi - t),$$

$$0 = \int_0^{2\pi} dt \ln(2R_0^2(1 - \cos(\phi - t)) \sin(\phi - t),$$

$$0 = \int_0^{2\pi} dt \ln(2R_0^2) \sin(\phi - t) + \int_0^{2\pi} dt \ln (1 - \cos(\phi - t)) \sin(\phi - t),$$

$$0 = \ln(2R_0^2)\,(\cos(\phi) - \cos(\phi - 2\pi)) + \int_0^{2\pi} dt \ln(1 - \cos(\phi - t)) \sin(\phi - t).$$

Now it only remains to show that $\int_0^{2\pi} dt \ln(1 - \cos(\phi - t)) \sin(\phi - t) = 0.$

Let us denote $u \equiv \cos(t - \phi)$, $v \equiv \ln(1 - u)$. Then one has

$$-\int_0^{2\pi} dt u' \ln(1 - u) = -u \ln(1 - u)\Big|_0^{2\pi} + \int_0^{2\pi} dt\, uu'(1 - u)^{-1} =$$

$$= -\int_0^{2\pi} dt\, uu'(1 - u)^{-1} = u\Big|_0^{2\pi} + \ln(1 - u)\Big|_0^{2\pi} = 0.$$

This is that we wanted to prove.

5. Summary

We analyze the pure vortical motion in nuclear systems excluding the usual approximation on smallness of the excitation amplitude and the additional assumptions on the shape of a nuclear system. The equations to describe a nonlinear plane nuclear vortex are presented in the frame of nuclear hydrodynamics. The evolution of the shape of a vortex is analogous to a propagation of a nonlinear dispersion wave in a plane. These states can be considered as a generalization of elliptic Kirchhoff vortex. A short qualitative analysis of the main features of the vortex is done.

We have shown that at the class of $C^1_{[0,2\pi]}$ functions the periodic solutions having the symmetry relative to the turn by an angle $2\pi/l$ with integer parameter $l = 2, 3, 4\ldots$ can exist and we have presented two such solutions. The expected vortexes are two-dimensional analogues to the rotating nuclear systems which have stable quadropole, octupole, hexadecupole deformations accordingly.

Our investigations of the elliptic Kirchhoff vortex in nuclear systems were stimulated by Prof. Ya.A.Smorodinsky.

References

1. Lukach I., Smorodinsky Ya.A. — JETP, 1969, 57, p.1324.
2. Aberg S. — Nucl. Phys., 1988, A488, p.147.
3. Zeldovich Ya.B. — Pisma v JETP, 1966, 4, p.78.
4. Bertsch G.F., Broglia R.A., Schrieffer R. — Nuovo Cimento, 1988, 100A, p.283.
5. Shapiro I.S. — Nucl. Phys., 1990, A518, p.73.
6. Fowler G.N., Raha S., Weiner R.M. — Phys. Rev., 1985, C31, p.1515.
7. Sandulescu A., Ludu A., Greiner W. — Int. Journ. of Mod. Phys., 1993, E1, p.1.
8. Kartavenko V.G. — CLUSTERS'93, 2nd Int. Conf., Santorini, Greece, 1993, p.63.
9. Khalatnikov I.M. — An Introduction to the Theory of Superfluidity, W.A.Behjamin, Inc., New York, 1965.
10. Hrapak A.G., Yakubov I.T. — Uspekhi Phys. Nauk, 1979, 129, p.45.
11. Moretto L.G., Tso K., Colonna N., Wozniak G.J. — Phys. Rev. Lett., 1992, 69, p.1884.
12. Kartavenko V.G. — Journ. of Phys., 1993, G19, p.L83.
13. Bauer W., Bertsch G.F., Shulz H. — Phys. Rev. Lett., 1992, 69, p.1888.
14. Lamb H. — Hydrodynamics, 6th Ed., Dover Publications, New York, 1932.
15. Kartavenko V.G. — Particles and Nuclei, 1993, 24, p.1469.

Received on March 3, 1994.

Краткие сообщения ОИЯИ №1[64]-94 *JINR Rapid Communications No.1[64]-94*
УДК 539.1.03+539.1.043+539.125.52

SPALLATION NEUTRON SOURCE WITH HARD ENERGY SPECTRUM FOR DETECTOR COMPONENT TESTING AT THE DUBNA SYNCHROPHASOTRON

A.D.Kovalenko, Yu.A.Panebratsev, V.I.Yurevich

A white neutron source has been recently constructed on the basis of the Dubna Synchrophasotron. A flux of neutrons with energies over the range up to several GeV is produced by spallation reactions using a pulsed proton/deuteron beam from the Synchrophasotron. The spallation neutron source on a Pb (W and ^{238}U in future) thick target has been intended for radiation damage studies of detector components of experimental setups at colliders.

The investigation has been performed at the Laboratory of High Energies, JINR.

Источник нейтронов с жестким энергетическим спектром для испытания компонент детекторов на дубненском синхрофазотроне

А.Д.Коваленко, Ю.А.Панебратцев, В.И.Юревич

Источник нейтронов с белым спектром был недавно разработан на базе дубненского синхрофазотрона. Поток нейтронов с энергиями до неск. ГэВ образуется за счет реакций расщепления ядер с использованием импульсного пучка протонов или дейтронов синхрофазотрона. Источник нейтронов расщепления на основе Pb (W и ^{238}U в будущем) толстой мишени предназначен для изучения радиационных повреждений компонент детекторов экспериментальных установок на коллайдерах.

Работа выполнена в Лаборатории высоких энергий ОИЯИ.

1. Introduction

Modern high luminosity colliders produce a high intensity field of secondary neutrons, charged hadrons and gamma-rays around an interaction point and at a large pseudorapidity region in experimental setups. The estimations show that the neutron fluence is up to $10^{13}-10^{15}$ n/cm^2 per year and determines the time of setup operation [1,2]. So, radiation damage studies are one of the main goals of the *R & D* stage of experimental setup design at colliders. The secondary neutrons have a hard energy spectrum overlapping a wide energy region up to several GeV. A neutron field with the same energy spectrum for detector component testing can be produced by the Spallation Neutron Source (SNS) based on an accelerator, where a proton/deuteron intermediate energy beam bombards a thick heavy metal target.

Some years ago the activity was begun on the creation of the radiation hardness test facility using several-GeV proton/deuteron beam of the Dubna Synchrophasotron [3—5]. First studies were carried out with various lead targets. The next step of source development is to reconstruct the SNS area around the Target-2 station and to use more compact targets from high density materials, W and ^{238}U.

2. Facility

A schematic plan view of the beam line with the experimental areas is shown in Fig.1. The proton/deuteron beam from the Synchrophasotron passes through a magnet system and then focuses at point F3 at Experimental Area 1 (EA1) where the Target-1 station is located with a neutron/charged hadron TOF spectrometer based on the detectors with plastic, stylben and NaJ(T1) scintillators. This spectrometer is used to obtain the energy spectra and yields of neutrons and charged hadrons emitted from various targets investigated and also to get the characteristics of neutron field of thick target as a prototype of the SNS located at the Target-2 station at the Experimental Area 2 (EA2) [6]. The beam comes to Experimental Area 2 (EA2) passing through next magnet system placed downstream Target-1. The beam hits neutron production Target-2 located at focus point F4 of the beam line where the experimental area is surrounded by a 3-m concrete shielding. There are two rotating arms with targets there, and one of them can be located at the beam line. After irradiation, the neutron production target can be turned away from the tested samples. A system of MWPCs and ionization chambers located upstream and downstream Target-1 and Target-2 measures the profile and intensity of the beam. The dimension of the beam spot on the front of the target in the vertical and horizontal directions is approximately 10 mm (FWHM). The beam has a time structure consisting of macropulses which can be of a various duration up to 400 ms in a different mode of beam burst. We expect to operate with approximately 8 macropulses/min with a beam intensity of up to $5 \cdot 10^{11}$ particles/macropulse. A new experimental method for neutron/hadron field mapping at accelerator-based facilities has been developed recently [7,8]. We are going to use this method for neutron field studies and an operative neutron flux control around Target-2 of the SNS. Brief information about experimental details of this technique is given in Appendix.

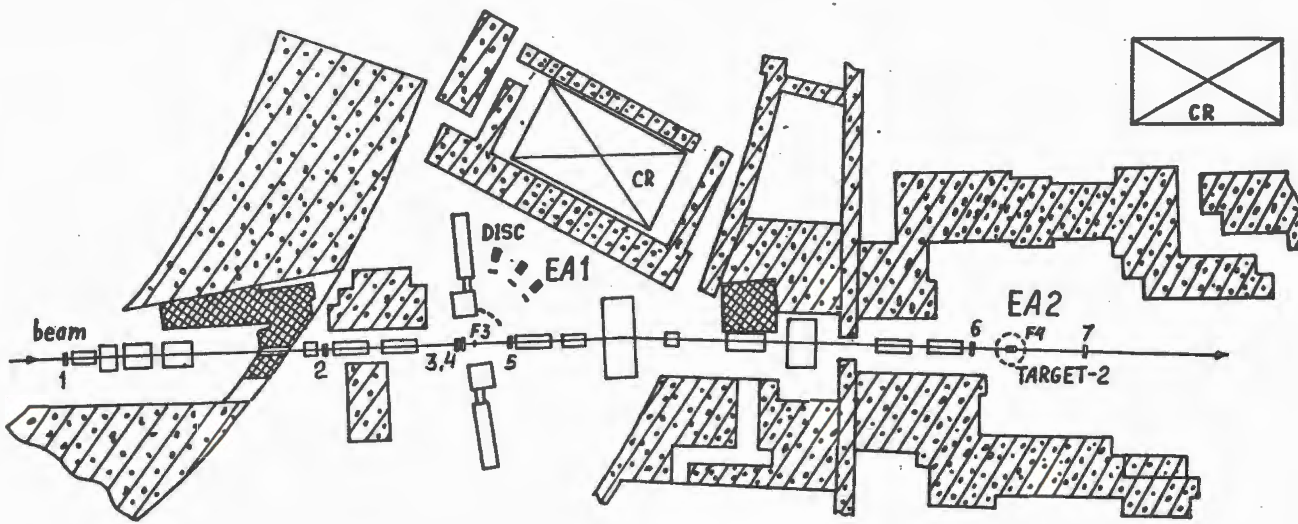

Fig. 1. A Schematic plan view of the Synchrophasotron beam line around the focus F3, F4: EA1, EA2 — Experimental Areas 1 and 2; CR — counting room; DISC — hadron spectrometer; 1,4—7 — MWPC; 2,3 — ionization chamber

3. Neutron Field of SNS Based on Lead Targets

In the last few years a lot of measurements with various thick lead targets irradiated by several-GeV protons/deuterons have been performed at the Dubna Synchrophasotron [3—5]. The energy spectra of neutrons for two lead targets 8 × 8 × 8 cm and ϕ20 × 20 cm measured by the TOF spectrometer at angles of 30, 90 and 150 deg. with 2.0- and 2.55-GeV proton beams are presented in Fig.2 and Fig.3, respectively. The obtained average energies of emitted neutrons for these are given in Table 1. A comparison of the energy spectra of the high-energy component of neutrons and charged hadrons for these targets is shown in Fig.4. The yield of charged hadrons is one order less than that of high-energy neutrons (the ratio of the yields depends on the emission angle) and approximately two orders less than the total neutron yield. All energy spectrum of neutrons and the spectrum of

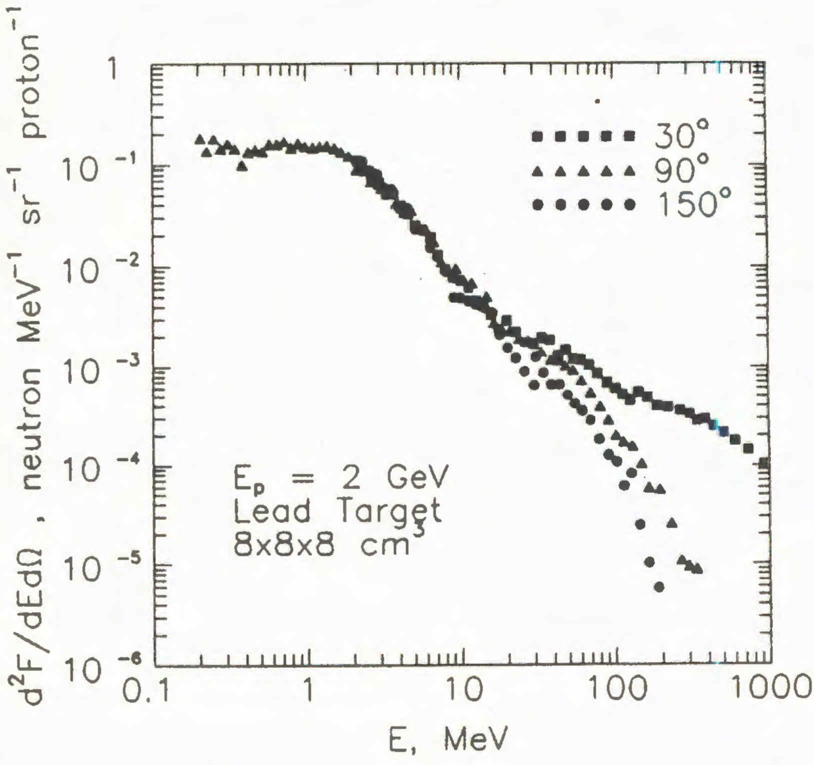

Fig.2. Energy spectra of neutrons for lead targer 8×8×8 cm bombarded by 2-GeV protons

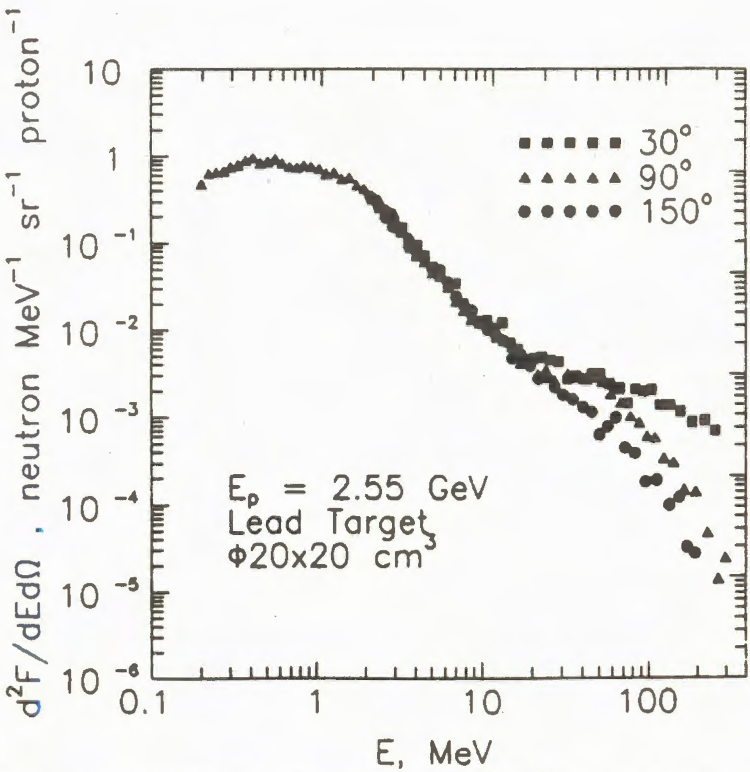

Fig.3. Energy spectra of neutrons for lead target $\phi 20 \times 20$ cm bombarded by 2.55-GeV protons

protons emitted at an angle of 90 deg. from the lead target $\phi 20 \times 20$ cm bombarded by 2.55-GeV protons is shown in Fig.5. A lot of measurements have been carried out with the threshold detector technique for an extended

Table 1. Average energy of neutrons (MeV)

Target (cm)	Beam	Energy (GeV)	Angle (deg.) 30	90	150
8×8×8	*p*	2.0	82.7	10.7	6.36
	d	2.0	29.5	8.12	4.53
ϕ20×20	*p*	2.55	21.6	7.31	4.38
	d	2.0	20.7	6.28	4.21

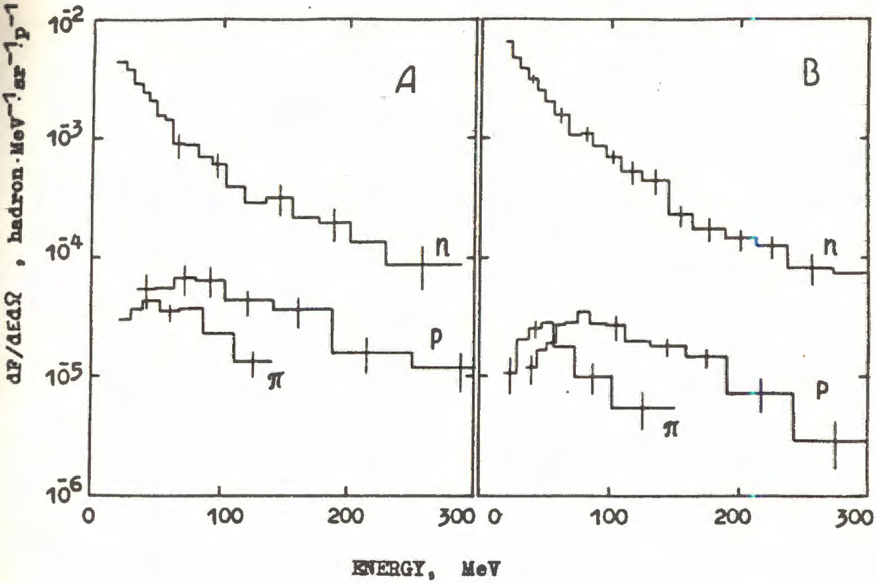

fig.4. Energy spectra of high-energy neutrons, protons and charged pions at angle of 90 deg. for two lead targets 8 × 8 × 8 cm (*A*) and ϕ20 × 20 cm (*B*) bombarded by 2.55-GeV protons

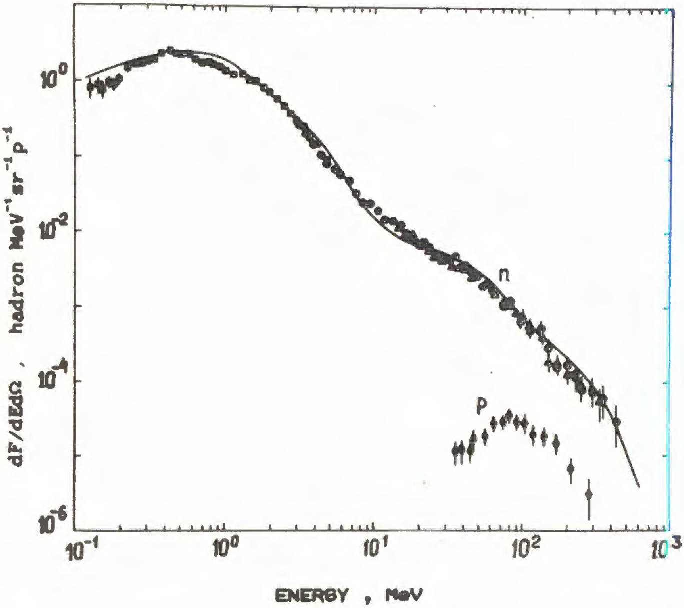

Fig.5. Energy spectra of neutrons and protons at angle of 90 deg. for lead target ϕ20×20 cm bombarded by 2.55-GeV protons

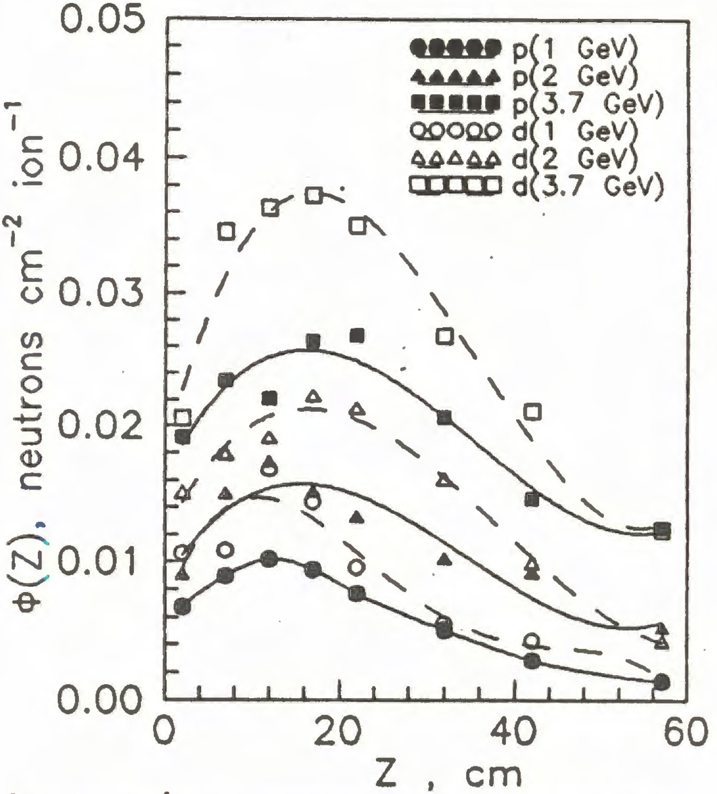

Fig.6. The distributions of neutrons along the side-surface of the lead target $\phi 20 \times 60$ cm bombarded by different energy protons and deuterons

Table 2. A dependence of the partial neutron yields for extended lead target $\phi 20 \times 60$ cm on an energy of proton/deuteron beam (n/p(d))

E_p (GeV)			E_d (GeV)		
1.0	2.0	3.65	1.0	2.0	3.76
All neutrons					
23.4 ± 3.0	44.2 ± 3.1	80.7 ± 6.9	26.2 ± 5.0	58.5 ± 8.2	98.9 ± 14.0
$E_n > 1$ MeV					
15.2 ± 2.1	27.5 ± 2.0	49.9 ± 4.5	14.6 ± 2.8	31.3 ± 4.7	56.6 ± 8.5
$E_n > 20$ MeV					
2.0 ± 0.3	4.7 ± 0.4	8.6 ± 1.0	1.8 ± 0.4	4.1 ± 0.7	8.2 ± 1.5

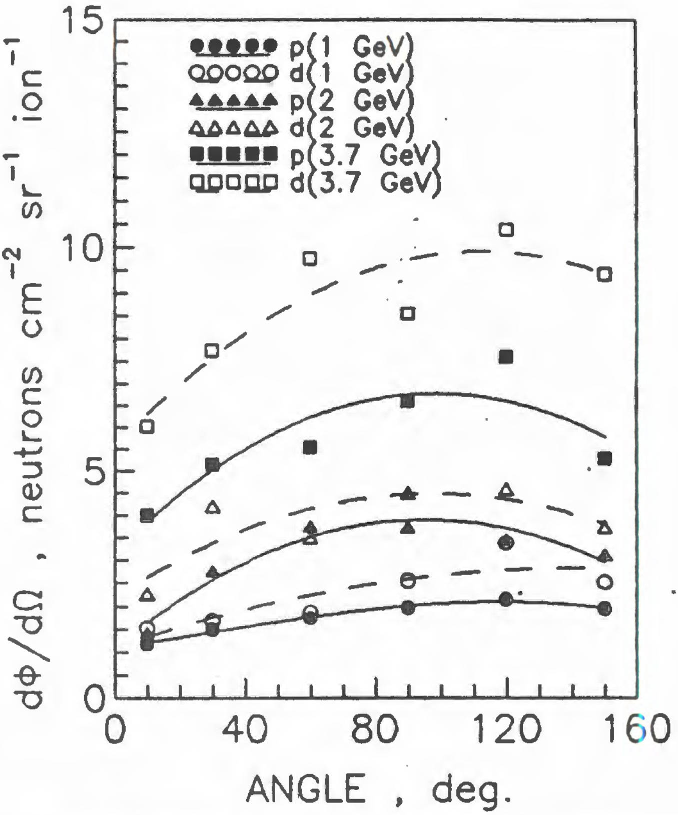

Fig.7. Angular distributions of neutrons for the lead target $\phi 20 \times 60$ cm bombarded by different energy protons and deuterons

Table 3. Average energy of neutrons emitted from extended lead target $\phi 20 \times 60$ cm

E_p (GeV)	$\langle E \rangle$ (MeV)	E_d (GeV)	$\langle E \rangle$ (MeV)
1.0	8.82	1.0	5.53
2.0	11.57	2.0	6.94
3.65	13.72	3.76	9.43

lead target $\phi 20 \times 60$ cm [3,4]. The side-surface and angular distributions of neutrons for 1—3.7-GeV incident projectiles are shown in Fig.6 and Fig.7, respectively. The angular distribution for different energy groups of neutrons obtained for 3.65-GeV protons is presented in Fig.8. The partial

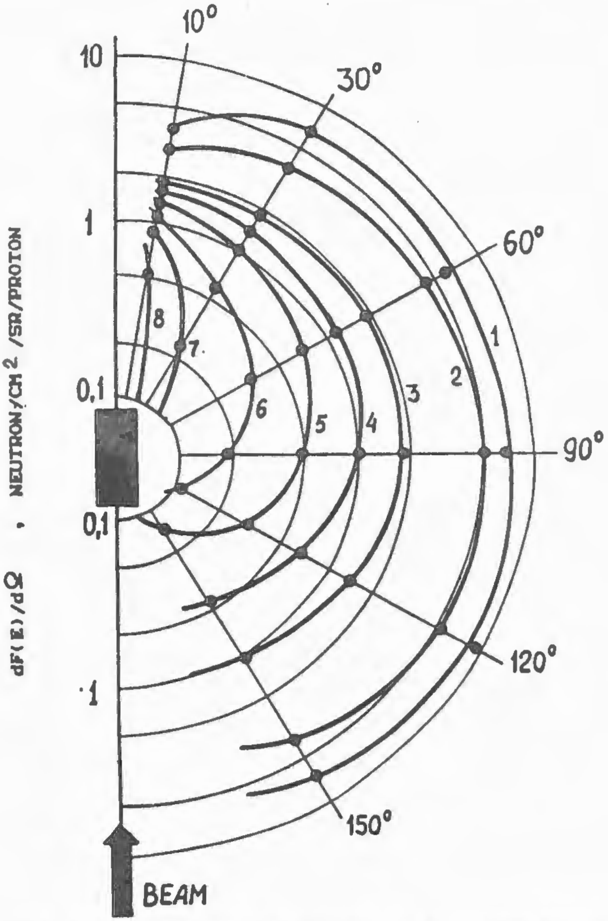

Fig.8. Angular distribution of neutrons in the different energy groups for the lead target $\phi 20 \times 60$ cm bombarded by 3.65-GeV protons. 1 — all neutrons; 2—8 — neutrons with the energy above 1, 6, 20, 50, 100, 250 and 500 MeV respectively

yields of neutrons for three energies of incident protons and deuterons and the average energies of neutrons emitted at the total solid angle are given in Table 2 and Table 3, respectively. The average energy rises with increasing the energy of beam particles and decreasing emission angle and target size. The total yield of neutrons per projectile approximately linearly depending on the kinetic energy of beam ions is ~ 145 n/p and ~ 180 n/d for 8-GeV projectiles, Fig.9.

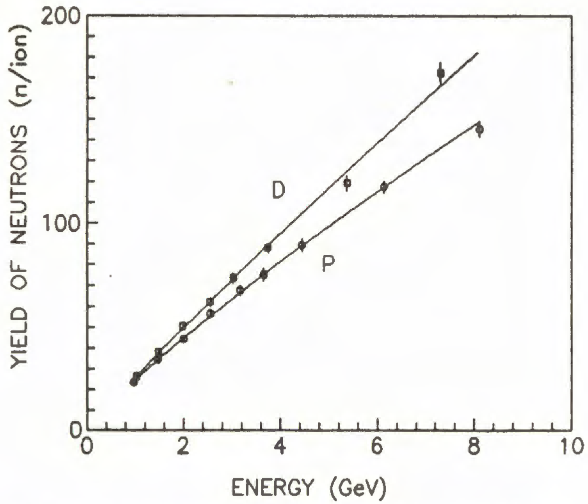

Fig.9. Energy dependence of the total neutron yield for lead target $\phi 20 \times 60$ cm bombarded by protons and deuterons

4. Neutron Flux Estimation

The estimation of the neutron flux for various neutron production targets has been carried out using the results of experimental studies and calculations for the 9-GeV/c proton beam with an intensity of $5 \cdot 10^{11}$ p/burst. Three types of targets (lead, tungsten or uranium-238 thick targets) for the reconstructed Target-2 station have been considered. These targets absorb about 80—90% of beam ions by inelastic interactions inside the target. The results of the estimation for different distances from the target are presented in Table 4.

Table 4. Neutron flux extimation for the neutron production targets

Distance from target	Target					
	Pb		W		^{238}U	
	$\frac{n}{cm^2\,burst}$	$\frac{n}{cm^2\,day}$	$\frac{n}{cm^2\,burst}$	$\frac{n}{cm^2\,day}$	$\frac{n}{cm^2\,burst}$	$\frac{n}{cm^2\,day}$
side-surface	$3 \cdot 10^{10}$	$3.4 \cdot 10^{14}$	$5 \cdot 10^{10}$	$5.6 \cdot 10^{14}$	$7.6 \cdot 10^{10}$	$8.6 \cdot 10^{14}$
20 cm	$1 \cdot 10^{10}$	$1 \cdot 10^{14}$	$1 \cdot 10^{10}$	$1 \cdot 10^{14}$	$1.7 \cdot 10^{10}$	$1.7 \cdot 10^{14}$
50 cm	$1.6 \cdot 10^{9}$	$1.6 \cdot 10^{13}$	$1.6 \cdot 10^{9}$	$1.6 \cdot 10^{13}$	$2.7 \cdot 10^{9}$	$2.7 \cdot 10^{13}$

The SNS based on the Dubna Synchrophasotron produce neutrons with a hard energy spectrum and a flux up to several $10^{14}\ n \cdot cm^{-2}\ day^{-1}$, and so one can see that this source represents a good facility for the radiation damage testing of detector components.

Appendix

Advanced Technique for Neutron Field Research and Operative Dose Control

Method	threshold detectors technique [5]	
Detector	set of fissile and fragmenting layers connected with SSNTDs[1] or TFBCs[2]	
Efficiency	$\leq 10^{-5}$	
Number of detectors in a single experiment	for SSNTD technique — up to 1000 and more for TFBC technique — up to 100 and more	
On-line data accumulation	for SSNTD technique — NO for TFBC technique — YES	
Data processing	for SSNTD technique — off-line for TFBC technique — on/off-line	Iteration procedure
Properties of detector system	small dimensions and weight (portable) simple electronics	
Dimensions of detector	for SSNTD technique — $\phi 30 \times 10$ mm for TFBC technique — $30 \times 15 \times 10$ mm	

[1] solid state nuclear track detector (6 μm PETP)
[2] thin-film breakdown counter (Si)

TFBC TECHNIQUE

Automated method for operative neutron flux and dose control with on-line data accumulation and processing by computer

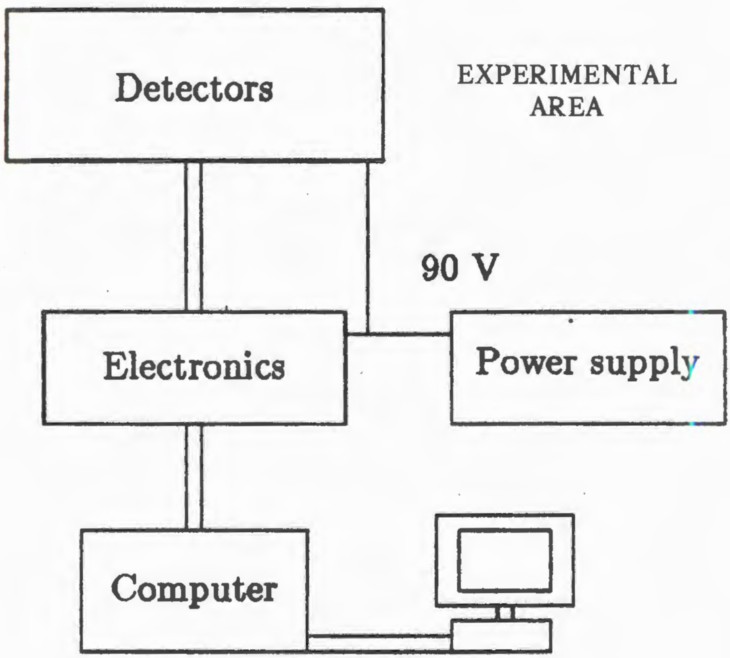

Data processing and showing spatial-energy map of neutron field (or dose map)

SSNTD TECHNIQUE

Semi-automated method for neutron field research

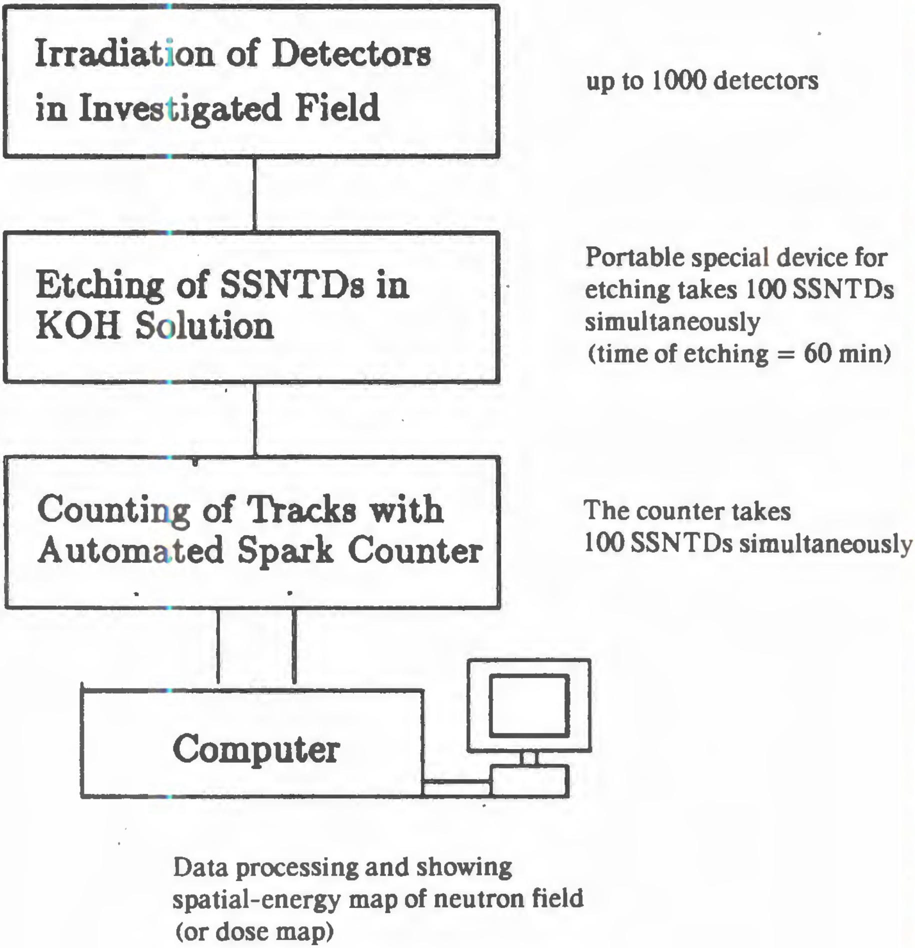

References

1. Proc. of the Symp. on Detector Research and Development for the Superconducting Super Collider, Oct. 15—18, 1990, Fort Worth, Texas, Ed. T.Dombeck, V.Kelly and G.R.Yost, World Scientific Publishing Co. Ptc.Ltd., 1991.
2. Large Hadron Collider Workshop Oct. 4—9, 1990, Aachen, Ed. G.Jarlskog and D.Rein, CERN 90-10, ECFA 90-133, 1990, vol.3.
3. Vassilkov R.G., Yurevich V.I. — Proc. ICANS-XI Meeting, 1990, KEK, Tsukuba, Japan, KEK 90-25, 1991, vol.1, p.340.
4. Nikolaev V.A., Yurevich V.I., Yakovlev R.M., Vassilkov R.G. — Proc. ICANS-XI Meeting, 1990, KEK, Tsukuba, Japan, KEK 90-25, 1991, vol.1, p.612.
5. Daniel A.V., Lyapin V.G., Tsvetkov I.O., Yurevich V.I., Yakovlev R.M. — JINR Report E1-92-174, Dubna, 1992.
6. Kovalenko A.D., Panebratsev Yu.A., Shimanskiy S.S., Yurevich V.I., Yakovlev R.M. — JINR Report E1-92-250, Dubna, 1992.
7. Vorobjev I.B., Nikolaev V.A., Yurevich V.I., Yakovlev R.M. — Nucl. Tracks Radiat. Meas., 1991, vol.19, p.541.
8. Yurevich V.I., Nikolaev V.A., Yakovlev R.M., Vassilkov R.G. — JINR Report E1-92-189, Dubna, 1992.

Received on February 1, 1994.

УДК 541.183

SIMULATION OF NON-EQUILIBRIUM SORPTION DYNAMICS OF THE INTERACTING PARTICLES

V.K.Fedyanin, I.V.Puzynin, Kh.T.Kholmurodov*

The set of two nonlinear equations which describes the gas sorption dynamics of nondissociative molecules is investigated. The results were obtained for different values of adatoms interaction energy. The comparison of three approximations in particle correlation effects is carried out.

The investigation has been performed at the Laboratory of Computing Techniques and Automation, JINR.

Моделирование динамики сорбции взаимодействующих частиц

В.К.Федянин, И.В.Пузынин, Х.Т.Холмуродов

Исследована система нелинейных уравнений, описывающая динамику сорбции газа недиссоциирующихся молекул. Результаты получены для различных значений энергии взаимодействия между сорбируемыми частицами. Приводятся сравнения результатов в рамках трех приближений учета корреляционных эффектов.

Работа выполнена в Лаборатории вычислительной техники и автоматизации ОИЯИ.

The processes within two or more phases play an essential role in a wide class of physical and chemical phenomena [1]. Here, first of all, one can include the adsorption and desorption processes. In this work we present the results on simulation of gas sorption dynamics taking into account the interaction between adatoms.

For the sorption dynamics of gas, which is transferred with the constant velocity, we have the following system of nonlinear equations:

$$v \frac{\partial \nu}{\partial \xi} + \frac{\partial \nu}{\partial \tau} + \frac{\partial \theta}{\partial \tau} = d \frac{\partial^2 \nu}{\partial \xi^2}, \quad (\tau = t/\tau_0), \tag{1}$$

$$\frac{\partial \theta}{\partial \tau} = \left(\frac{\nu}{a p_0} - 1 \right) f(\theta), \quad (\nu = n\gamma), \tag{2}$$

*Tajik State University, Dushanbe

$$\nu(\xi, \tau = 0) = 0,\ \theta(\xi, \tau = 0) = 0,\ 0 \le \xi \le k_1, \tag{3}$$

$$\nu(\xi = 0, \tau) = \nu_0,\ \nu(k_1, \tau) + c\frac{\partial\nu(k_1, \tau)}{\partial\xi} = 0,\ 0 \le \tau \le k_2. \tag{4}$$

Here ν is dimensionless gas concentration, θ — cover in terms of adsorption $(0 < \theta < 1)$, a is the adsorption coefficient, p_0 — the equilibrium pressure corresponding to the surface coverage θ, and $f(\theta)$ expresses the correlation effects between adatoms.

The equation (2) is obtained on the basis of the Hamiltonian for adsorbat-adsorbent open system [2],

$$H = -\mu\sum_f N_f - \varepsilon\sum_{\langle fg\rangle} N_f N_g,$$

where ε is the effective adatoms interaction parameter ($\varepsilon > 0$ corresponds to physical adsorption; $\varepsilon < 0$, to chemisorption), μ is the effective chemical potential, $N_f = 0,1$, respectively, means the free and the occupied active center on surface. It is to be noted that $\theta = \langle N_f \rangle$, and, on the other hand, θ unambiguously defines the mean value of sorbat concentration in the sorbent pores.

The equation (2) is the kinetic equation for the monolayer coverage

$$\frac{\partial\theta}{\partial t} = v_{ads} - v_{des}, \tag{5}$$

where v_{ads} and v_{des} are, respectively, the adsorption and the desorption velocities.

To derive the equation (2) we used the expressions v_{ads} and v_{des} for nondissociative (one-central) adsorption and desorption [3]:

$$v_{ads} = r_A f(\theta),\ v_{des} = r_D f(\theta), \tag{6}$$

$$r_A = \frac{J^* P\exp(-\beta(\varepsilon_k - \varepsilon_0))}{J_0 h a p_0},\ r_D = \frac{J^*\exp(-\beta\varepsilon k)}{J_a h\beta}, \tag{7}$$

Here $J*$, J_0 and J_a are, respectively, statsums of activated complex, of the particles in a gas phase and in adsorbate, P is the pressure in adsorptional systems, ε_0 and ε_k are the adatom binding and the adsorption activation energies, $\beta = (k_B T)^{-1}$, h is the Planck constant (for ideal gas to be adsorped we have $P\beta = n$).

Thus taking into account the formulas (6)—(7) one can obtain from (5) the equation which can easily be reduced to the form of (2):

$$\frac{\partial\theta}{\partial t} = \frac{1}{\tau_0}\left(\frac{P\beta\gamma}{ap_0} - 1\right) f(\theta),$$

where $\tau_0 = \dfrac{J_a h\beta}{J_*}\exp(\beta\varepsilon_k)$ have the time dimension and $\gamma = \dfrac{J_a}{J_0}\exp(\beta\varepsilon_0)$ have the dimension inverse to concentration and it connects the statsums of the molecules in the gas phase and in the adsorbate.

The expressions for ap_0 and $f(\theta)$ are concretized for the different approximations in particle correlation effects (e.g., molecular field approximation (MFA), polynomial fission (PF), quasichemical approximation (QCA) and so on). In particular, in QCA we have [4]:

$$\frac{1}{ap_0} = \frac{1-\theta}{\theta}\,[1 - r + r\exp(-\beta\varepsilon)]^{-z}, \tag{8}$$

$$r = \frac{\delta - 1 + 2\theta}{\delta + 1},\quad \delta = \sqrt{(1-2\theta)^2 + 4\theta(1-\theta)\exp(\beta\varepsilon)},$$

$$f(\theta) = \theta(1 + yr)^z,\quad y = \exp(\beta(\varepsilon_1 - \varepsilon)) - 1.$$

We solved the set of equations (1)—(4) numerically. For the numerical solution we used the following difference scheme [5]:

$$\frac{\nu_m^{n+1} - \nu_m^n}{\Delta\tau} + \nu\frac{\nu_m^{n+1} - \nu_{m-1}^{n+1}}{\Delta\xi} = -F(\nu_m^n, \theta_m^n),$$

$$\frac{\theta_m^{n+1} - \theta_m^n}{\Delta\tau} = F(\nu_m^n, \theta_m^n),$$

$$F(\nu_m^n, \theta_m^n) = \left(\frac{\nu_m^n}{ap_0} - 1\right) f(\theta_m^n).$$

As an initial approximation we consider the stationary values of the coverage, i.e., $\dfrac{\partial\theta}{\partial\tau} = 0$. In this case for the given distribution of the gas concentration we have the isotherm $\theta = \theta(\nu)$. The numerical results for the fixed values of the particles interaction energy ε (eV) and the temperature

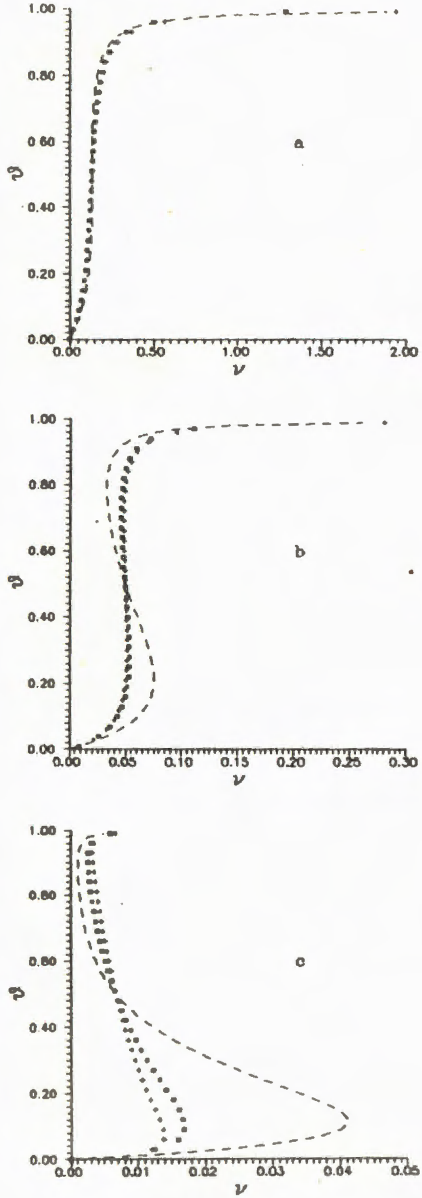

Fig.1. The sorption isotherms for $\beta\varepsilon$ = 1.0(a), 1.5(b) and 2.5(c).

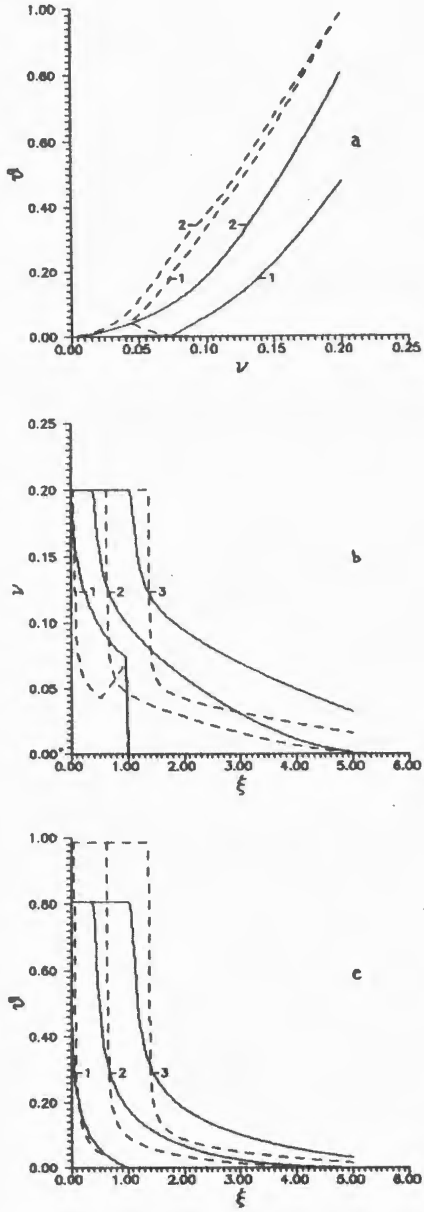

Fig.2. The sorption isotherms of dynamical equations (1)—(4) for $\beta\varepsilon$ = 1.0(- -) and 1.5 (—).

of the system $\beta = (k_B T)^{-1}$ (eV)$^{-1}$, such that $\beta\varepsilon = 1.0$, 1.5 and 2.5, are, respectively, shown in Fig.1a, b and c.

The results for the QCA, i.e. the computations with the formulas (8), are drawn by markers ^^^. In Fig.1, for comparison, the results obtained in the approximation of PF (the signs "+") and in MFA (the dashed line) are also plotted. The results show that with the increase of the adatoms interaction parameter $\beta\varepsilon$ the sorption isoterms become essentially nonlinear.

In Fig.2a, b and c we present the results of the direct solutions of the equations (1)—(4) for non-equilibrium sorption dynamics (the solid lines for $\beta\varepsilon = 1.0$, the dashed lines for $\beta\varepsilon = 1.5$). The evolutions of $\nu(\xi, \tau)$ and $\theta(\xi, \tau)$ (Fig.2b and c) in the interval $\xi \in [0,5]$ are shown at three moments: 1 — for $\tau = 1.0$; 2 — for $\tau = 5.0$; 3 — for $\tau = 10.0$. The Tables 1 and 2 give a convergence of the difference scheme applied with the Runge rule [6]:

$$\sigma = \frac{Y_i(\Delta\tau) - Y_i(\Delta\tau/2)}{Y_i(\Delta\tau/2) - Y_i(\Delta\tau/4)} .$$

Table 1. The convergence of the numerical values of θ

ξ	$\theta(\Delta\tau)$	$\theta(\Delta\tau/2)$	$\theta(\Delta\tau/4)$	σ
2.0	0.1798875	0.1816078	0.1824608	2.016764
4.0	0.0564381	0.0569365	0.0571856	2.000803
6.0	0.0140383	0.0142581	0.0143684	1.992747
8.0	0.0012153	0.0012625	0.0012865	1.966666
9.0	0.0001261	0.0001348	0.0001393	1.933333

Table 2. The convergence of the numerical values of ν

ξ	$\nu(\Delta\tau)$	$\nu(\Delta\tau/2)$	$\nu(\Delta\tau/4)$	σ
2.0	0.0939182	0.0943445	0.0945539	2.035817
4.0	0.0490738	0.0493528	0.0494917	2.008639
6.0	0.0182292	0.0184387	0.0185435	1.999045
8.0	0.0025861	0.0026634	0.0027025	1.976982
9.0	0.0004115	0.0004328	0.0004438	1.936353

Conclusions

1. The equation for external diffusive kinematics of gas sorption is obtained. The sorption dynamics of the interacting particles is investigated.

2. The numerical analysis of the sorption equations and the convergence of the difference scheme is carried out.

3. The nonlinear behaviour of the sorption isotherms depending on adatoms interaction parameters is found.

References

1. Nicolis G., Prigogine I. — Exploring Complexity. W.H.Freeman and Company, New York, 1989, p.313.
2. Fedyanin V.K. — J.Chem.Phys., 1972, 46, No.1, p.119 (in Russian).
3. Tovbin Yu.K., Fedyanin V.K. — Kinetika i kataliz, 1978, 19, 4, p.989 (in Russian).
4. Tovbin Yu.K., Fedyanin V.K. — Kinetika i kataliz, 1978, 19, 5, p.1202 (in Russian).
5. Samarskiy A.A., Popov Yu.P. — The Difference Method for Solution of the Gasodynamic Problems. M.: Nauka, 1992, p.423 (in Russian).
6. Kalitkin N.N. — Numerical Methods. M., Nauka, 1978, p.457 (in Russian).

Received on February 28, 1994.

УДК 539.1.074.3

EFFECT OF PULSE TIME GATE ON CsI(Tl) LIGHT OUTPUT

A.S.Fomichev, I.David, S.M.Lukyanov, Yu.E.Penionzhkevich, N.K.Skobelev, O.B.Tarasov

The mass and charge identification of secondary particles with $Z < 4$ by a large CsI(Tl) scintillation detector is performed using the pulse shape analysis and the time-of-flight methods. The dependence of light output on E, A and Z is studied in an energy range of 1—20 MeV/A and special attention is paid to the integration time of the photo multiplier anode signal. It is found that the behaviour of the calibration curves strongly depends on the choice of the integration time interval.

The investigation has been performed at the Flerov Laboratory of Nuclear Reactions, JINR.

Влияние сигнального временного окна на световой выход CsI(Tl)

А.С.Фомичев и др.

Представлена массовая и зарядовая идентификация вторичных частиц с $Z < 4$ большим сцинтилляционным детектором на основе CsI(Tl) с помощью анализа формы импульса и времяпролетного метода. Исследовалась зависимость светового импульса от E, A и Z в диапазоне энергий 1—20 МэВ на нуклон, специальное внимание при этом уделялось времени интегрирования анодного сигнала фотоумножителя. Было установлено, что поведение калибровочных кривых сильно зависит от выбора временного интервала интегрирования.

Работа выполнена в Лаборатории ядерных реакций им.Г.Н.Флерова ОИЯИ.

1. Introduction

The light output of the same inorganic crystals BaF_2, NaI(Tl), CsI(Tl) as an explicit function of E, A, Z has a strong dependence on integration time interval. It is explained by a different pulse form of front and tail, essentially for the light charged particles with $Z < 4$ [1].

Storey et al. [2] showed that the light output of the scintillator could be described by a sum of two exponential functions with the fast and slow components:

$$L(t) = h_f/\tau_f \exp(-t/\tau_f) + h_s/\tau_s \exp(-t/\tau_s). \qquad (1)$$

On the basis of properties of the crystal luminescence: i) with decreasing ionisation density, the ratio $R = h_s/(h_f + h_s)$ strongly increases and ii) the fast component τ_f is an increasing value as the ionisation density of the particle decreases, a good identification of E, A, Z for $Z < 4$ is obtained using the pulse shape analysis (*PSA*), i.e. measurement of the amounts of charge in two regions of the anode pulse [3—5]. Sophisticated understanding of the behaviour of rise and decay times of light pulse versus particle type provides a substantial help for optimisation of the *PSA* conditions. However, accurate measurements of the light output as a function $F(E, A, Z, t)$ in case of low energies are very poor because there is difficult particle identification and large energy error. Really, these measurements are possible if the energy of particle is fixed using a magnetic spectrometer. In this work the dependence of light output on time interval, over which the anode current signal of the photo multiplier was integrated is studied for light secondary particles with $Z = 1—3$ in the energy range of 1—20 MeV/A.

2. Experimental Procedure

The main characteristics of CsI(Tl) counter with a crystal diameter of 200 mm and a thickness of 15 mm coupled by a hollow light guide to the photomultiplier have been determined in ref. [5,6]. The present investigation is based on the possibility to detect secondary beams produced in reaction ^{11}B(20 MeV/A) + ^{181}Ta using the U-400 (FLNR, JINR) cyclotron when the energy of particles is fixed and known exactly on a magnetic spectrometer. The identification of the products in this case, by the pulse shape analysis is shown in Fig.1 (a) at a magnetic rigidity B_ρ = 1.32 Tm. It is noticed that the proton peak is out of $Z = 1$ systematics because the 15 mm thickness of CsI(Tl) crustal can't keep them from stopping. Changing a magnetic rigidity B_ρ from 0.81 Tm up to 1.35 Tm secondary particles are measured at energies of E = 1—20 MeV/A. In this energy range the CsI pulse height is investigated for $^{1-3}$H, $^{3-6}$He and $^{6-9}$Li isotopes versus time intervals T_1(0.0; 0.4 μs), T_2(0.0; 2.0 μs), T_3(1.5; 2.0 μs) of the anode signal. Both T_1 and T_2 gates are started well before the pulse rise and have a duration of 0.4 μs, 2.0 μs respectively, while T_3 window has a delay line equal to 1.5 μs. Particle identification is carried out using the *PSA* and *TOF* methods as shown in ref. [6] and Fig.1 (a,b) with the standard *LeCroy* electronics ADC 2249W and TDC 2228A.

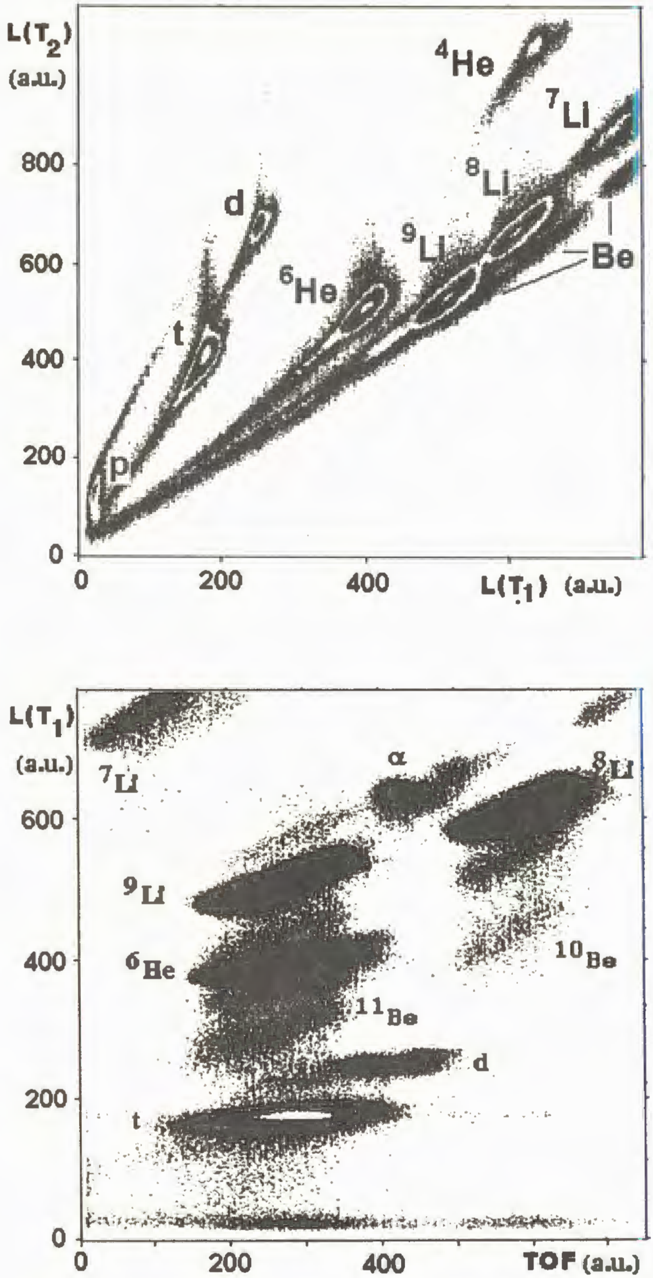

Fig.1. The identification of secondary particles emitted in the ^{11}B(20 MeV/A) + ^{181}Ta reaction by a) PSA and b) time-of-flight methods

3. Results

The light output measurements for three integration intervals reflecting the front (T_1) and the tail (T_3) of light pulse and also their mixing (T_2) are presented in Fig.2.

First, we are concerned with the charge dependence of the light output for different integration time windows. It is known that with the increase of Z of the detected particle the total light output expressed as $L = h_f + h_s$ decreases because the ratio $h_s/(h_f + h_s)$ increases with decreasing ionisation density. This behaviour can be clearly seen in Fig.2c where the light output integrated in the time window T_3 is shown. With its window the slow light component dominates and, as a rule, it is weaker for higher Z. This fact also is confirmed by the plot resulting from the integration over interval T_1 (see Fig.2a). Within this time interval, where the fast light component plays the dominant role, the behaviour of calibration curves is quite reversed. The results point out that for higher Z the contribution of the fast light component dominates that is in a full agreement with the statement made above.

The same interplay of the slow and fast light components is observed for the mass dependence of light output for the given Z. As an example, the absolute values of light output for ^{3}He, ^{4}He, ^{6}He ions are increasing for the first interval and decreasing for the third one. As the T_2 window (Fig.2b) includes both the fast and slow components, this interval is not very suitable for identification and the calibration curves can hardly be separated.

In the same way the mass dependence of the light output is studied. The relative mass dependence ΔL of light output of a triton and proton gives 21% and 16% for T_1 and T_2, respectively, at $E_t = 30$ MeV. However, there is almost no difference ($\Delta L \sim 2\%$) for the time interval T_3 like in ref. [7], where a spectroscopy amplifier operates with a 3 μs shaping time. On the other hand, for particles with $Z = 2$, the difference of the ^{6}He, ^{4}He light outputs results in a variation of 6% and 8% in ΔL for T_1 and T_3, respectively, at energy $E = 55$ MeV of ^{6}He. For T_2, the difference amounts to less than 4%. The front edge of the pulse (the integration in T_1) does not allow to separate different Li isotopes. Nevertheless, if slow component participates in integration, as it is in (T_2) or (T_3), our procedure starts to separate ^{9}Li and ^{7}Li at energy of about 40 MeV. At higher energies ΔL further increases and reaches a value of about 8% at $E = 80$ MeV.

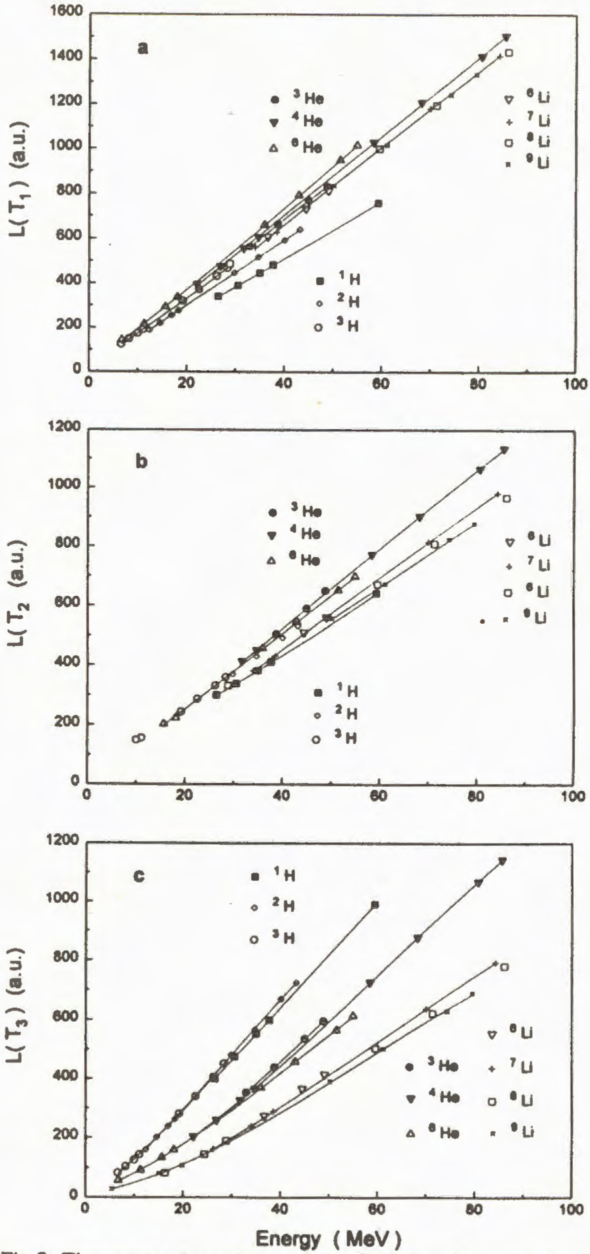

Fig.2. The energy dependence of the CsI(Tl) light output for particles with $Z = 1$—3 produced in ^{11}B(20 MeV/A) + ^{181}Ta reaction at low energies: a) the time integration interval $T_1(0.0; 0.4\,\mu s)$; b) — $T_2(0.0; 2.0\,\mu s)$; c) — $T_3(1.5; 2.0\,\mu s)$.

The fact that the behaviour of the calibration curves differs, if integration is done within two separate time intervals, enables one to use the CsI(Tl) detector for the good particle identification. The pulse shape analysis is applied and for different time interval combinations the matrices (T_1, T_3) and (T_1, T_2) have been compared earlier [6]. Since in T_2 both the fast and slow components are present, the combination with T_2 gives a slightly worse identification, which agrees well with the data presented in ref. [4].

Moreover, one should note (Fig.2) that non-linear effects of calibrated curves are essentially different in T_1 and T_3 intervals. $L(T_1)$ can be practically described by a linear function of energy as $L(T_1) \sim \gamma E + \beta$, where γ and β denote the slope and the intercept, respectively, while the light output in T_3 $L(T_3) = \gamma E + \beta\,\{\exp(-\alpha E) - 1\}$ has the outstanding non-linear dependence of energy especially in the region of $E < 5$ MeV/A. These results are in fairly agreement with measurements of Benrachi et al. [4] where it is shown that the relative intensity of the slow component increases as a function of energy and that the fast pulse decay is slower as the energy increases.

4. Conclusion

The response of CsI(Tl) scintillator to light ions ($Z = 1$—3) separated by a magnetic spectrometer is studied in this work at the energies of 1—20 MeV/A. To optimise the *PSA* condition special attention is paid to the choice of integration time intervals. It is found that the relative light output and nonlinear effects of the calibration curves strongly depend on the delay line and gate duration. One can conclude that the edge part of the pulse (T_3) is very suitable for the energy calibration of hydrogen isotopes because there is scarcely any difference between p, d, t signals. On the contrary, the particles with $Z = 3$ fall on a single straight line in T_1 window. Finally, the light output for helium isotopes is essentially distinctive in all studied intervals.

Reference

1. Birks J.B. — The Theory and Practice of Scintillation Counting. Pergamon, Oxford, 1964.

2. Storey R.S., Sack W., Ward A. — Proc.Phys.Soc.London, 1958, 72, p.1.
3. Alarja J. et al. — Nucl.Instr. and Meth., 1986, A242, p.352.
4. Benrachi F. et al. — Nucl.Instr. and Meth., 1989, A281, p.137.
5. Wagner W. et al. — JINR Rapid Com. 4[61]-93 Dubna, 1993, p.49.
6. Fomichev A.S. et al. — Preprint GANIL P-93-23, 1993; to be published in Nucl.Instr. and Meth.A.
7. Horn D. et al. — Nucl.Instr. and Meth., 1992, A320, p.273.

Received on March 9, 1994.

УДК 539.126.3

ON THE RADIAL EXCITATIONS OF THE LIGHT MESONS

Yu.I.Ivanshin

The difficulties of theoretical considerations of radial excitations of the light mesons are discussed. It is suggested to perform the partial-wave analysis of the experimental data on the diffractive $K\pi\pi$ production in the effective mass region of 900—1200 MeV to obtain the information on the first K-meson radial excitation.

The investigation has been performed at the Laboratory of Particle Physics, JINR.

Радиальные возбуждения легких мезонов

Ю.И.Иваньшин

Обсуждается проблема радиальных возбуждений легких мезонов. Предлагается провести парциально-волновой анализ экспериментальных данных по дифракционному $K\pi\pi$ рождению в области эффективных масс 900—1200 МэВ с целью получения сведений о первом уровне радиального возбуждения K-мезона.

Работа выполнена в Лаборатории сверхвысоких энергий ОИЯИ.

At present there is a great amount of experimental data on diffractive production of $K\pi\pi$ system everywhere in the world. The author emphasizes the necessity to perform the partial-wave analysis (PWA) of the data wherever they exist to get an information which should witness the existence of radially excited K-meson in the $K\pi\pi$ effective mass region 900—1200 MeV. The suggestion has the following grounds.

In the last years the radial excitations of light mesons (π and K) have been discovered in the experiments on diffractive production of 3π and $K\pi\pi$ systems at different energies. For instance, in the 5-th joint CERN—JINR experiment (Bologna—Dubna—Milan collaboration) at the IHEP accelerator the reactions

$$\pi + A \to 3\pi + A$$

and

$$K + A \to K\pi\pi + A$$

were investigated in 1977—1984. The PWA has been performed in the mass region above 900 MeV for 3π and above 1100 MeV for $K\pi\pi$ systems. The reason to begin analysis from 900 and 1100 MeV is historical: the PWA initially was performed to look inside A_1 and A_3 «bumps» in 3π system (A_1 starts from 900 MeV), and Q_1 and Q_3 «bumps» in $K\pi\pi$ system (Q_1 starts from 1100 MeV). Two resonances $\pi(1240)$ and $\pi(1770)$ in the 3π system with the quantum numbers of the pion [1] and one resonance $K(1460)$ in the $K\pi\pi$ system with the quantum numbers of K-meson [2], have been observed. Resonances $\pi(1240)$ and $K(1460)$ have been interpreted as 2^1S_0 states — the first radial excitations of π- and K-mesons, accordingly. The other groups (see [3] or [4], for example) have presented the PWA in the same region.

In 1985 a relativistic quark model of hadron states was developed and compared with the experimental data [5]. But the above mentioned assignment of the $\pi(1240)$ as 2^1S_0 state to tune parameters of the model, created a problem to identify the 2^3S_1 state — the first radial excitation of ρ-meson: the ρ level predicted by the model at 1450 MeV, was not compatible with the data. Moreover, to obtain a sensible fit the authors were made attribute masses 150 MeV to pion and 470 MeV to kaon instead of real masses.

Another approach ($\pi(1240)$ is considered as 3^1S_0 state — that is as the second radial excitation of pion) was suggested in paper [6]. In this case the model requires that there should be one more pion radial excitation level with a mass in the region 700—800 MeV.

The recently performed partial-wave analysis of the data on diffractive 3π-production in the effective mass region 600—900 MeV has shown [7] that indeed there is an indication of existence of a new radially excited state in the 3π system with a mass 749 ± 30 MeV and width 32 ± 17 MeV.

For $K\pi\pi$ states the model [5] predicts the state $K(1450)$ as the first radial excitation of kaon if the 3π state $\pi(1240)$ is considered as the first radial excitation of pion. But the same model with the $\pi(749)$ as 2^1S_0 state, will identify the $K(1460)$ of ref. [2] as 3^1S_0 state and will require new additional resonance 2^1S_0 which should be the first radial excitation in the $K\pi\pi$ system.

One can hope that the PWA of the existing data in the region 900—1200 MeV will give an indication on existence of this resonance. If it is so it should be desirable to come back to experiment and collect more $K\pi\pi$ data, concentrating attention (with the help of a more strict trigger system, for instance) in the region below 1200 MeV.

The author greatly appreciates the encouragement of Prof. I.A.Savin and Prof. A.A.Tyapkin and sincerely thanks Dr. V.A.Petrov and Dr. I.M.Vasilevsky for useful discussions.

References

1. Belline G. et al. — Phys.Rev.Lett., 1982, 48, p.1697.
2. Tyapkin A. — Nucl.Phys., 1992, 25B, p.52.
3. Daum C. et al. — Nucl.Phys., 1981, B182 3, p.269.
4. Bityukov S.I. et al. — Proc. IV International Conference on Hadron Spectroscopy. Washington, College Park, Maryland, 1991 , p.51.
5. Godfrey S., Isgur N. — Phys.Rev., 1985, D32, p.189.
6. Ivanshin Yu.I. et al. — JINR Comm. P2-83-727, Dubna, 1983.
7. Ivanshin Yu.I. et al. — JINR Prep. E1-93-155, Dubna 1993 (submitted to «Phys. Lett. B»).

Received on February 22, 1994.

УКАЗАТЕЛЬ СТАТЕЙ К СБОРНИКАМ «КРАТКИЕ СООБЩЕНИЯ ОИЯИ», №№ 1[58]—6[63], 1993

№ 1[58]

№ 2[59]

№ 3[60]

№ 4[61]

№ 5[62]

№ 6[63]

JINR RAPID COMMUNICATIONS — 1993
CONTENTS

No.1[58]

No.2[59]

No.3[60]

No.4[61]

No.5[62]

No.6[63]

ИМЕННОЙ УКАЗАТЕЛЬ К СБОРНИКАМ «КРАТКИЕ СООБЩЕНИЯ ОИЯИ» №№ 1[58]—6[63], 1993

AUTHOR INDEX 1993